Stability and transport properties of multiple-patch quasi-equilibria

Stability and transport properties of multiple-patch quasiequilibria

R. M. Schoemaker, H. J. H. Clercx, and G. J. F. van Heijst
Department of Physics, Eindhoven University of Technology, P.O. Box 513, 5600 MB Eindhoven, The Netherlands

(Received 28 November 2003; accepted 11 June 2004; published online 1 September 2004)

A novel subclass of exact solutions to the Euler equations in two dimensions has been put forward recently [D. Crowdy, "A class of exact multipolar vortices," Phys. Fluids **11**, 2556 (1999)]. The solutions show vortical equilibria which can be described by only two parameters. The first one designates the multipolar aspect of these equilibria, i.e., the number of point vortices involved, while the other parameter signatures the shape of the finite area of uniform vorticity in which the point vortices are embedded. The main aspect of these equilibria is that the vortical configuration is static, meaning that the velocity induced at the patch edge, outside the vortical area, and also at the locations of the point vortices is zero. We show with numerical experiments that quite remarkably the linearly stable equilibria of Crowdy seem to mix very efficiently in contrast to the unstable vortex solutions. In the second part of this paper we report on the dynamics, stability, and mixing properties of similar vortex systems where the point vortices are regularized to vortex patches (with uniform vorticity). Several of these multiple-patch vortices turn out to be remarkably stable, although the regularization itself should be considered as a (symmetric) perturbation of Crowdy's multipolar solutions. © *2004 American Institute of Physics*. [DOI: 10.1063/1.1785111]

I. INTRODUCTION

A class of exact multipolar vortices for two-dimensional (2D) Euler flows has been put forward recently by Crowdy.[1] These solutions show a family of equilibria that is described by only a few parameters. The vortical system comprises a certain number of point vortices (a central point vortex and n satellite point vortices) embedded in a finite area of uniform vorticity (referred to as "patch"). Provided that n is fixed, the shape of this finite area of uniform vorticity is determined by the distance of the satellite point vortices to the central point vortex, and the shape parameter is denoted by a (a more precise definition of a is given in the Appendix). As an example consider the triangular vortex ($n=3$) with $a=1.371$ and $a=2.0$ as shown in Fig. 1. A certain combination of a and n, together with a specified value of the strengths of the point vortices and the uniform vorticity of the patch (yielding zero total circulation of the multipolar vortex) results in a steady solution of the 2D Euler equations. For a complete mathematical problem definition of these multipolar vortex equilibria the reader is referred to Crowdy.[1]

The more general system of point vortices embedded in a vorticity patch has been observed in the so-called Penning–Malmberg trap used in plasma physics, where magnetized electron columns in a magnetic confinement are modeled as extremely small line vortices in a magnetic background field (see the experimental, numerical, and analytical studies by several investigators in recent years[2–6]). The patterns, the so-called vortex crystals,[7] that appear through self-organization in such a circular symmetric 2D flow setting can be described by analytical and numerical techniques that are mathematically equivalent to the 2D Euler equations. The multipolar vortex equilibria proposed by Crowdy[1] represent a special class of exact solutions to the 2D Euler equations. These equilibria are completely shielded, implying a nontrivial vorticity distribution for patch and point vortices. Moreover, these equilibria are steady, nonrotating structures. Crowdy and Cloke[8] have investigated the stability properties of these special solutions by imposing a perturbation on the positions of the point vortices. This symmetric perturbation consisted of relative displacements of $\mathcal{O}(10^{-1})$ of the point vortices, either radially inward or radially outward, from their equilibrium positions compared to the $\mathcal{O}(1)$ size of the vortex itself (note that, in the stability study by Crowdy and Cloke, small numerical errors seed the growth of any linearly unstable modes resulting ultimately in an asymmetrical decomposition of the vortex equilibria). Besides a linear stability analysis, the nonlinear evolution of the flow has been investigated as well with contour dynamics studies.[8–10] The work of Crowdy and Cloke[8] is consistent with the results of Morikawa and Swenson[11] in the limit $a\rightarrow\infty$ when one expects the patch boundary to have little effect and the polygonal array of point vortices, which are all bunched around the center of the near-circular patch, to behave as in the Morikawa and Swenson pure-point vortex problem. Note, however, that for finite values of a the presence of the patch boundary makes the analysis conducted by Crowdy and Cloke[8] much more complicated and its contribution to the stability properties becomes important as a decreases from infinity.

The exact multipolar equilibria can be perturbed by the displacement of point vortex positions, contour perturbations, or patch and/or point vortex strength variations. The stability analysis of Crowdy and Cloke[8] contains perturbations by means of small symmetric displacements of point vortex locations. One of the prime conclusions in these investigations is that the tripolar solution is unstable under all conditions. In the following section we investigate by means

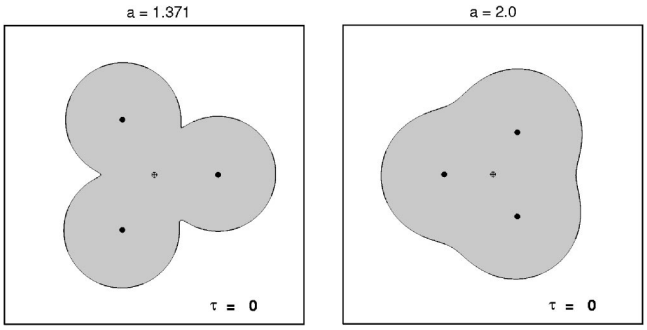

FIG. 1. The triangular vortex ($n=3$) with $a=1.371$ (left panel) and $a=2.0$ (right panel). The position of the central point vortex is denoted by an open circle with a +, and the satellite point vortices by filled circles.

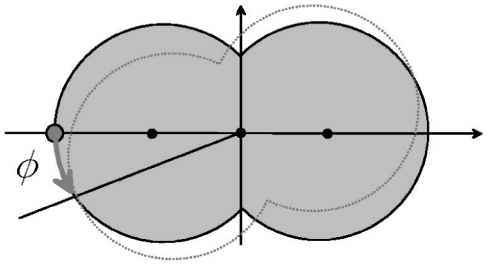

FIG. 2. Schematic of the definition of the phase shift ϕ for the perturbation of the bounding contour for the case of a tripolar vortex ($n=2$).

of a combined Point Vortex/Contour Dynamics (PVCD) algorithm the stability properties of the tripolar vortex, the triangular vortex, and the square vortex. Two different types of perturbations are employed. The first type consists of minute perturbations of the boundary of the vortex, resulting in a small residual velocity at the point vortex locations (Sec. II). The evolution of the perturbed multipolar equilibria are similar to those reported by Crowdy and Cloke,[8] and we will only briefly summarize our findings (including the rather remarkable mixing properties of such multipolar equilibria as found in our numerical experiments). The second type is based on replacing each point vortex by a finite uniform patch of vorticity with the same circulation as the original point vortex, and is discussed in Sec. III. Formulated in a slightly different way, the point vortices of Crowdy's solutions are in this case regularized to vortex patches, and the resulting vortex structures are probably "close" to equilibrium. There is, however, no *a priori* reason to assume steadiness of this kind of solutions of the 2D Euler equations. We would like to emphasize that we did not perform (and do not report on) a detailed mathematical and numerical search for precise multiple-patch quasiequilibria close to the point-patch equilibria introduced by Crowdy.[1] Finally, we briefly summarize our conclusions in Sec. IV.

II. INSTABILITY INDUCED BY CONTOUR PERTURBATIONS

The first part of this study concerns the effect of contour perturbations applied to the bounding contour of Crowdy's multipolar vortex equilibria. The perturbations in our investigations consist of sinusoidal disturbances that have very small amplitudes ε_0 relative to the length of the contour bounding the vortex. An initial contour perturbation is described according to

$$\varepsilon = \varepsilon_0 \sin\left(2\pi m \frac{\ell}{L} - \phi\right), \tag{1}$$

and ε refers to a normal displacement of the contour. In this expression, m represents the wave number, and ϕ the phase shift (with respect to a predetermined appropriate point at the contour). The amplitude of the perturbation is chosen as either $\varepsilon_0=10^{-3}$ or $\varepsilon_0=10^{-2}$. The parameters ε_0, m, and ϕ describe the shape of the sinusoidal perturbation uniquely (Fig. 2). The parameter L is the length of the contour enclosing the patch, and ℓ is a length variable that describes the appropriate location for the amplitude along the contour. This perturbation is actually a redistribution of uniform vorticity. The change in area of the patch is very small and scales linearly with ε_0. Therefore, ε_0 is kept sufficiently small. The minute change in patch distribution induces very small flow velocities at the bounding contour and at the point vortex locations after a first integration in time. Note that at the point vortex locations and at the contour the velocity is zero in the unperturbed vortex equilibrium. The minute velocities, introduced at the point vortex locations, will consequently advect them. The perturbation parameters ε_0, m, and ϕ together with the equilibrium parameters n and a, determine the evolution of the vortex. For more details on the role of these parameters on the instability process we refer to Schoemaker.[12]

The numerical experiments in this section include a class of perturbations that are more general than those considered by Crowdy and Cloke.[8] These authors deliberately restrict attention (in both their linear stability analysis and their nonlinear calculations) to purely irrotational perturbations. The perturbations embodied in Eq. (1) modify the patch area slightly ($\varepsilon_0 \ll 1$) and hence represent rotational perturbations.

The computations are performed with the PVCD method. The inclusion of the point vortex equations (for a proper mathematical formulation of point vortex systems see, e.g., Batchelor[13] and Aref[14]) in the contour dynamics algorithm yields a method for simulating flows of patches and point vortices with the same accuracy as ordinary contour dynamics simulations. For an overview of the mathematical formulation and numerical implementation of algorithms for contour dynamics, which can nowadays be considered as standard numerical techniques, the reader is referred to the works and reviews by Zabusky *et al.*,[9] Dritschel,[10] and Pullin.[15] The PVCD algorithm differs in the sense that not only contour-to-contour interactions are involved but three more interactions as well, i.e., contour-to-point vortex interactions (the induced velocity at the point vortex location due to the vorticity patch), point vortex-to-contour interactions (the induced velocity at all contour nodes due to the point vortices), and point vortex-to-point vortex interactions. A point vortex is implemented as a contour with only one node, having a finite circulation. The induced velocity field through the combination of these two approaches is still a full solution of the Euler equations. Furthermore, because of the singular character of the point vor-

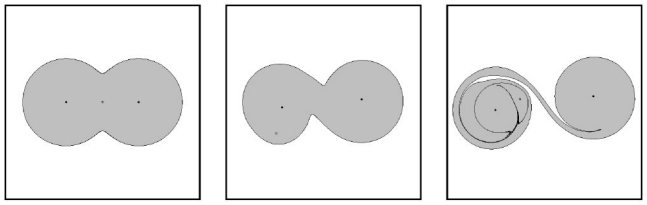

FIG. 3. An example of the nonlinear evolution of the tripolar vortex ($n=2$).

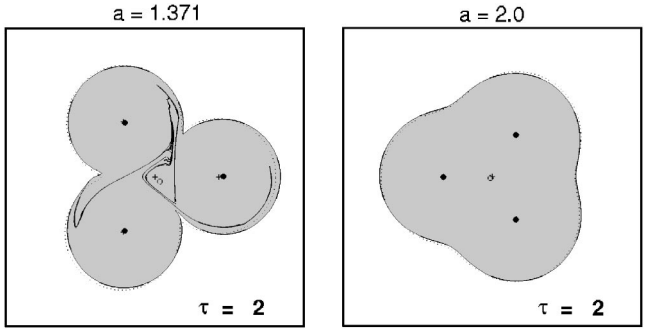

FIG. 4. A snapshot of the evolution of the triangular vortex ($n=3$) in case of a mode-2 perturbation with amplitude $\varepsilon_0=10^{-2}$. Left panel, $a=1.371$; right panel, $a=2.0$. The initial position of the point vortices is denoted by +. The actual positions of the point vortices at $\tau=2$ is denoted by an open circle (central point vortex) and filled circles (satellite vortices). The equilibrium position of the bounding contour is indicated by the dotted curve.

tex, the initial conditions of the flow at hand should be such that nodes of contours should not be placed too close to point vortices. Obviously, one should also avoid placing two or more point vortices too close to each other. The time step for the time integration scheme should be taken very small in those cases, thus yielding inefficient simulations.

In Crowdy and Cloke[8] the tripolar solution was found to be unstable for all $1<a<\infty$, when the positions of the satellite point vortices are perturbed by a relative displacement of $\mathcal{O}(10^{-1})$ from their equilibrium position. Note that, more generally, the Crowdy tripole is unstable to any infinitesimal perturbation (of any arbitrarily small size) that slightly displaces the central vortex. The contour perturbations in this section have a maximum initial amplitude of $\varepsilon_0=10^{-3}$ and $\varepsilon_0=10^{-2}$. For the tripolar solution and for all other multipolar equilibria, the central point vortex, which has a much smaller vorticity than the satellite point vortices, is of uttermost importance for the system to be in equilibrium. For the tripolar vortex a slight induced velocity at the central point vortex location will render the system immediately unstable for all perturbations and for all a.

The nonlinear evolution of the unstable tripolar configuration is characterized by the formation of new stable coherent structures. Figure 3 shows the evolution of the tripolar vortex for the $a=1.5$ equilibrium. Clearly, depending on the initial phase ϕ of the perturbation (1) of the bounding contour, the very weak central point vortex wanders off to one of the satellite regions. The major difference between the strength of the central point vortex and the satellite point vortex ($|\Gamma_s| \gg |\Gamma_c|$ for the values of a considered in this study, with Γ_c and Γ_s the circulation of the central and satellite vortex, respectively[1]) results in a strongly asymmetric dipolar structure and hence in a twisting displacement. A continued computation, with the dipole making another full turn, shows the formation of many (folded) filamentary structures. Accurate computation of the evolution of the vortices and the filaments requires a large amount of nodes (no contour surgery has been applied), and this prohibits a further computation with the parameter settings used in this study. The remaining circular area of uniform vorticity combined with the embedded point vortex evolves as a shielded Rankine vortex.

The solution with $n=3$ marks the triangular vortex with its four vortex extrema (see Fig. 1). This vortex equilibrium is found to be stable for the perturbations of order $\varepsilon_0=10^{-2}$ in case of the $a=1.371$ and $a=2.0$ equilibrium. The first value of a represents the case with the strength of the central point vortex equal to zero. The equilibrium is then maintained through a delicate balance between the uniform patch and the polygon of satellite point vortices.[8] A snapshot of the flow evolution is given in Fig. 4 for an $m=2$ mode perturbation for $a=1.371$ (left panel) and $a=2.0$ (right panel). The positions of the point vortices and the overall shape of the configuration have not changed substantially—the uniform vorticity patch keeps its initial shape, but a major difference can be observed in the evolution of the bounding contour.

The above observations are further substantiated with the aid of Fig. 5(a), where we have plotted the quantity

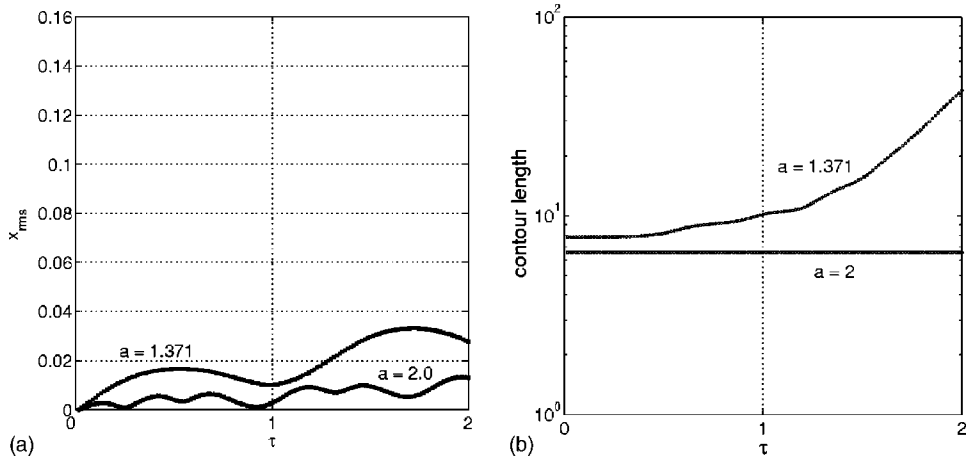

FIG. 5. Graphs illustrating the evolution of the triangular vortex structures shown in Fig. 4. (a) The rms values for the point vortex position deviations x_{rms}, see Eq. (2), in the course of time. (b) The evolution of the length of the bounding contour of the vortex patch.

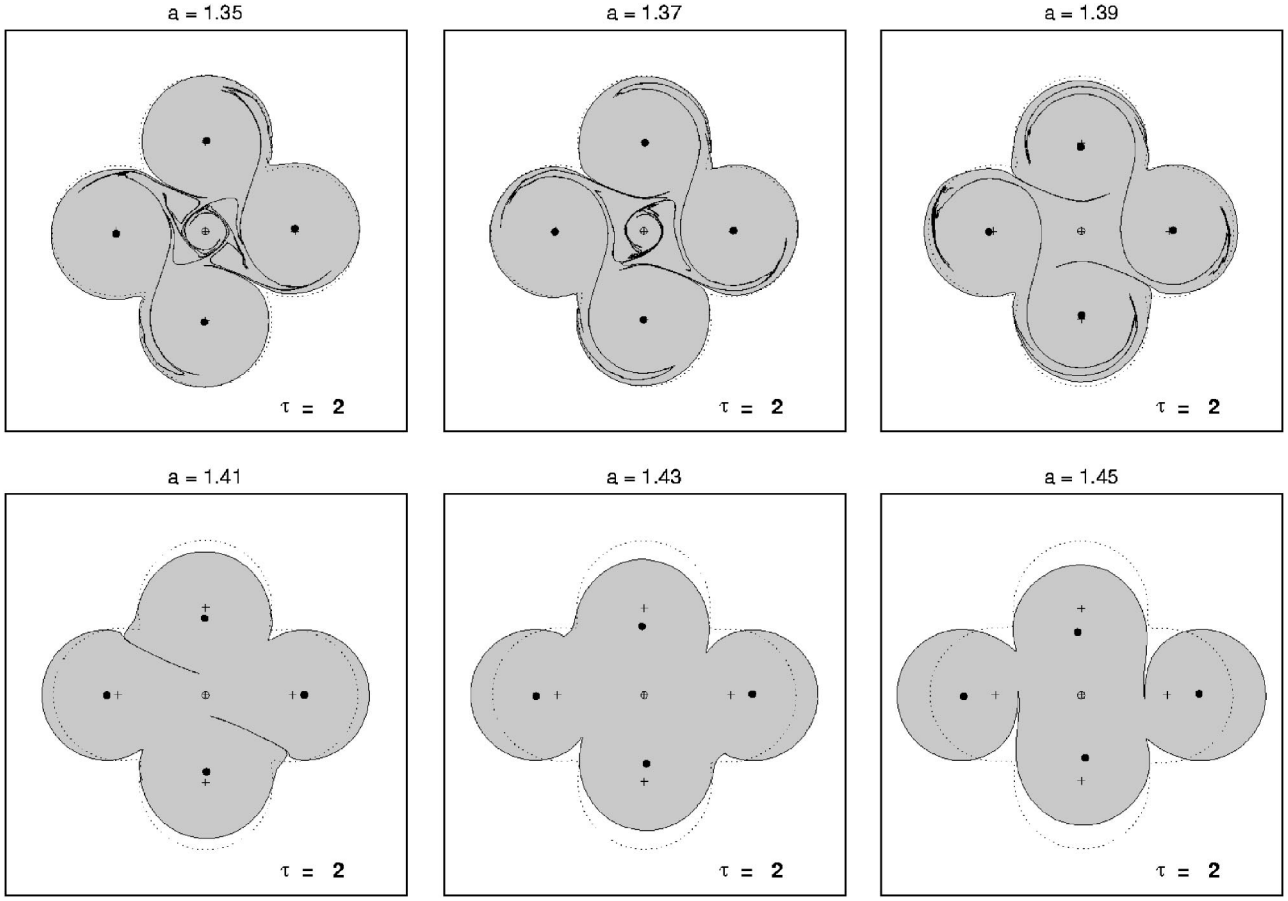

FIG. 6. Snapshots of the evolution of a square ($n=4$) vortex for $a=1.35$, 1.37, 1.39, 1.41, 1.43, and 1.45 at $\tau=2$. The initial positions of the point vortices are denoted by +. The actual positions of the point vortices at $\tau=2$ is denoted by an open circle (central point vortex) and filled circles (satellite vortices). The equilibrium (unperturbed) position of the bounding contour is indicated by the dotted curve.

$$x_{\mathrm{rms}} = \sqrt{\frac{1}{n+1}\sum_{i=1}^{n+1} |\mathbf{x}_{\tau,\mathbf{i}} - \mathbf{x}_{0,\mathbf{i}}|^2}, \tag{2}$$

which is the root mean square (rms) value of the position deflections $\mathbf{x}_{\tau,\mathbf{i}}-\mathbf{x}_{0,\mathbf{i}}$ of the $n+1$ point vortices at time τ. The rms value during and at the end of the simulation for both vortices (with $a=1.371$ and $a=2.0$) is very small compared to the scale of the vortex, which is $\mathcal{O}(1)$. We conclude therefore that the results of these two simulations are in agreement with the analyses and conclusions stated in Crowdy and Cloke,[8] i.e., for $n=3$ and $1.211<a<\infty$ the triangular vortex is stable for linear perturbations.

Before proceeding with further results a few comments should be made to elucidate the meaning of the unit time ($\tau=1$). An eddy turnover time $\mathcal{T}=2\pi/\omega$, with ω the uniform vorticity of the patch, can be introduced. For the tripolar vortex we use the uniform patch $\omega\approx 6$, thus $\mathcal{T}\approx 1$. The unit time $\tau=1$ thus corresponds approximately to an eddy turnover time. The integration time step depends on the actual velocities (or vorticities) and the node distribution. As a rule of thumb[16] the time step during integration is $\Delta\tau\approx\pi/10\omega = \frac{1}{20}\mathcal{T}$, or, referring again to the tripolar vortex, $\Delta\tau\approx 0.05$. Similar estimates can be made for the triangular and square vortices.

Another aspect is the variation in the length of the contour in the course of time [see Fig. 5(b) where a semilogarithmic plot of the contour length increase in the course of time is shown], which can be considered as a local measure of mixing. The transport of the passive tracers (the material contour) is quite substantial for the $a=1.371$ vortex. The increase in contour length does even show an exponential rate at later times, which—as can be seen in Fig. 4(a)—is illustrated by the (folded) material contour that is advected throughout the entire vortex. The $a=2.0$ triangular vortex, on the other hand, does not show substantial transport of fluid initially located near the boundary at all.

The square vortex, marked by $n=4$, is interesting for its stability and transport properties when a certain interval for values of a is investigated. The analysis in Crowdy and Cloke[8] shows a threshold for the shape parameter a for this solution to be stable in case of perturbations of the point vortex positions. They found that for each $1.241<a<1.4$ the vortex is stable, where $a=1.241$ is the limiting case below which no physical solutions exists (for $n=4$). We have numerically investigated the effect of contour perturbations for the interval of $a=1.35,\ldots,1.47$ with steps of 0.02. The mode number of the imposed perturbation is $m=2$, the amplitude is $\varepsilon_0=10^{-2}$, and the initial phase shift is $\phi=0.65\pi$. In Fig. 6 all end frames at $\tau=2$ are shown. The results for $a<a_{\mathrm{stab}}\approx 1.4$,

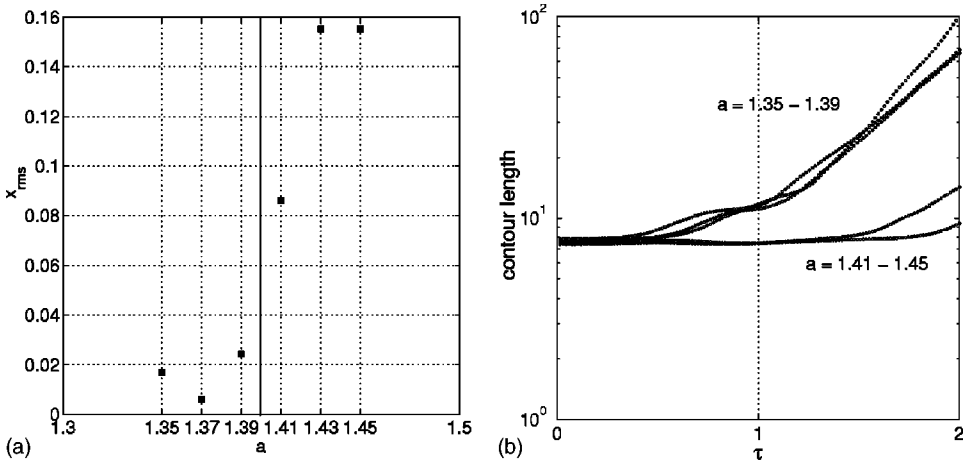

FIG. 7. Graphs illustrating the evolution of the square vortex structures shown in Fig. 6. (a) The rms values x_{rms}, see Eq. (2), for the satellite position deviations at $\tau=2$. The solid vertical line marks the stable/unstable regime. (b) The evolution of the length of the bounding contour of the vortex patch.

the upper three frame shots, show a stable configuration for the overall shape of the vorticity distribution and the point vortex positions. Despite the strong contour folding, indicating substantial mixing, the overall distribution of the uniform vorticity does not deviate substantially from its initial allocation. This behavior indeed shows that in case of contour perturbations the square vortex is stable for values smaller than $a=1.4$.

For a discussion of the evolution beyond the threshold value we inspect the three lower frame shots shown in Fig. 6. Here a similar advection of the material contour into the vortex area is observed, be it that the time for the perturbed flow to enter this stage lasts much longer and is less severe (less transport in the boundary region). More important are the displacements of the satellite point vortex locations. The vortical equilibria for $a>1.4$ are unstable in the sense that the distribution of uniform vorticity is disturbed in such a way that two opposite point vortices move inward and the other two satellites move outward, indefinitely. A simulation up to $\tau=3$ has been conducted for the case with $a=1.45$. This run confirms the scenario that the patch will ultimately be destroyed: the central point vortex starts to move to one of the satellite vortices (and many filaments have been formed). Moreover, the evolution shows symmetry breaking in a similar way as shown by Crowdy and Cloke.[8] The higher the value for $a>a_{\mathrm{stab}}$ is, the sooner the vortex breaks up.

The observations in Fig. 6 are further substantiated by quantitative measurements of the point vortex positions and the contour length. Figure 7 shows the rms values for the point vortex position deviations, as defined by Eq. (2), at the end of the simulation in the left picture. The stable behavior is confirmed by very small rms values of the satellite deflections in the course of time. The value for $a=1.41$ seems to be situated in a transition regime between the stable and the unstable regime. A clear division between the stable and unstable regimes is apparent in these contour perturbation experiments. For the evolution of the contour length, given in the semilogarithmic plot in Fig. 7(b), this division is even more distinct. The experiments with $a<1.4$ show a strong folding of the contour, and the length of these contour increases exponentially after $\tau=1$. In the time interval $1\leqslant\tau\leqslant 2$, the length increases by one order of magnitude and the (folded) contour is advected throughout the entire vortex area. For $a>1.4$, the evolution of the contour postpones its lengthening and does so only when the vortex breaks up.

We conclude, therefore, that the numerical experiments verify that the square vortex is stable for $a\lesssim 1.4$ and unstable for $a\gtrsim 1.4$ for the case of contour perturbations. Furthermore, in the stable regime the transport of the material tracers (the contour nodes) leads to exponential stretching rates in the course of time and covers the entire vortex. For the unstable regime ($a\gtrsim 1.4$) a variation in the contour length is measured after the vortex breaks up, while the rate of increase in length is higher for larger a.

III. MULTIPLE-PATCH VORTICES

The equilibria investigated in the former section demand the use of point vortices embedded in a specially shaped patch of uniform vorticity. In this section we diverge from the point vortex description and investigate an approach to the vortex equilibria: we replace the point vortices with circular patches of uniform vorticity in such a way that the circulation of each new embedded patch is identical to that of the replaced point vortex. It is expected that these generalized vortical structures are probably close to equilibrium in some sense. It is not our aim, however, to find a detailed mathematical and numerical formulation for precise multiple-patch quasiequilibria close to the point-patch equilibrium of Crowdy.[1]

This change into a so-called multiple-patch vortex is expected to have consequences for the dynamics of the flow and can be seen as a perturbation to the generic point-patch equilibrium introduced by Crowdy.[1] We would like to emphasize, however, that the present disturbance is symmetric with respect to the center of the vortex (a brief discussion of slightly off-centered patches is provided in Sec. III A), but this symmetric disturbance yields vortices that can be considered as regularized versions of the Crowdy equilibria. In a generic (Crowdy) equilibrium the velocity is zero at the contour and at the point vortex locations. In case of a multiple-patch vortex, however, the uniform distribution of vorticity of each patch is in a way influenced by the induced velocities in the area occupied by the patch. The question at hand is,

TABLE I. The patch size settings for the three vortex systems. The runs that were carried out are indicated by a × (and the − means that no such runs have been conducted). See text for further details.

r_{vp} (% of r_s)	$n=2$	$n=3$	$n=4$
0	×	×	×
6.25	−	×	×
10	×	−	−
12.5	×	×	×
15	×	−	−
25	×	×	×

TABLE II. Numerical experiments were performed for the a values in this table.

$n=2$	$n=3$	$n=4$
$a=1.5$	$a=1.211$	$a=1.241$
$a=2.0$	$a=1.25$	$a=1.35$
	$a=1.371$	$a=1.37$
	$a=1.5$	$a=1.39$
	$a=2.0$	$a=1.41$
		$a=1.43$
		$a=1.45$
		$a=1.477$
		$a=1.5$
		$a=2.0$

what is the influence the induced flow has on each patch and on the system in general, i.e., do these multiple-patch vortex systems have similar stability characteristics as the point-patch equilibria? What is the dynamics of these (symmetrically) regularized Crowdy vortices? Are they in equilibrium anyway? Furthermore, how is the advection of passive tracers in these multiple-patch systems modified compared with the advection properties of point-patch equilibria? The objective is to address some of the above questions through numerical studies of the three multipolar systems already introduced in the former section: the tripolar vortex ($n=2$), the triangular vortex ($n=3$), and the square vortex ($n=4$). Various values for a will come into view by means of numerical experiments done with the contour dynamics method.[9,10,15,17] We characterize the dynamics and stability of the symmetrically regularized Crowdy vortices and measure the advection properties of these vortex structures by systematically monitoring the variation in length of particular contours of one or more vorticity patches. Lengths of strategically placed passive contours, i.e., contours that designate a patch with zero vorticity, are also monitored in the course of each simulation.

An important parameter is the radius of each embedded circular vorticity patch, denoted by r_{vp}. A similar parameter is the radius of the passive contours r_{pc}, which will be placed inside the bounding contour, yet outside the embedded patches (thus $r_{pc}>r_{vp}$). A characteristic length scale for the vortex is given by r_s, which is defined as the distance of the origin of the vortex to the center of a satellite patch. The patch radius r_{vp}, and the passive contour radius r_{pc} are defined as a percentage of r_s and the values for r_{vp} are given for several cases in Table I. The patches are equal in size for each quasiequilibrium, and the distance r_s is equal for each satellite and unique for a quasiequilibrium. Passive contours with radii according to the same values as in Table I are added to the center region of the vortex provided that $r_{pc}>r_{vp}$. An extra passive contour at $r_{pc}=0.5\,r_s$ is, however, added. For the satellite region only passive contours at $r_{pc}=0.25\,r_s$ and $r_{pc}=0.50\,r_s$ are added. Anticipating on the identical flow dynamics in each satellite region, due to the symmetry properties of the multiple-patch vortices, we implement the passive contours only for one satellite region. Note that the contour of the patch itself acts as a passive tracer which can be taken into account.

The various values of a for the three multiple-patch vortices (with $n=2$, 3, and 4, respectively) are tabulated in Table II. For measuring the length of each contour for each combination of a, n, and r_{vp}, a large number of numerical experiments is necessary. In order to quantify the characteristics of these flows in an efficient manner we introduce another parameter A, defined as the amplification factor

$$A \equiv \frac{L_c(\tau)}{L_c(0)}, \tag{3}$$

which designates the ratio of the contour length $L_c(\tau)$ after a certain time τ with the contour length $L_c(0)$ at the start of the simulation. This amplification factor A is then tabulated in a diagram for each simulation.

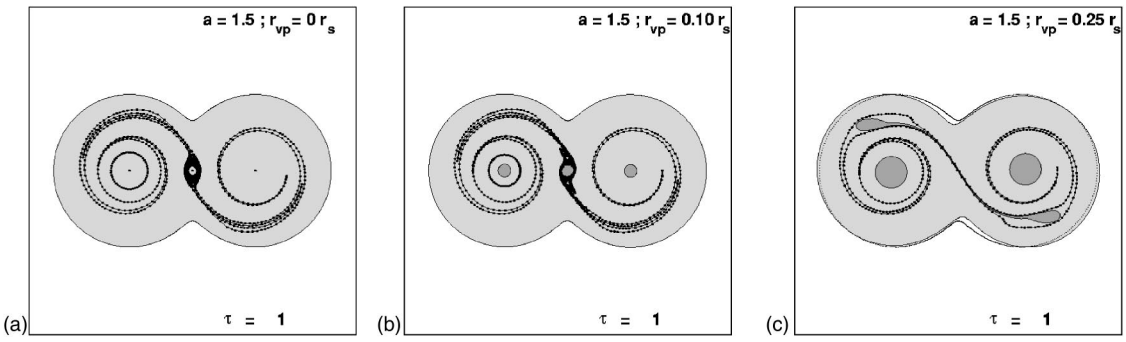

FIG. 8. Snapshots of the evolution of the $a=1.5$ tripolar system ($n=3$) at $\tau=1$ with (a) $r_{vp}=0$, (b) $r_{vp}=0.10r_s$, and (c) $r_{vp}=0.10r_s$. The gray and dark gray areas represent the vorticity patches, and the black dots designate the passive tracers.

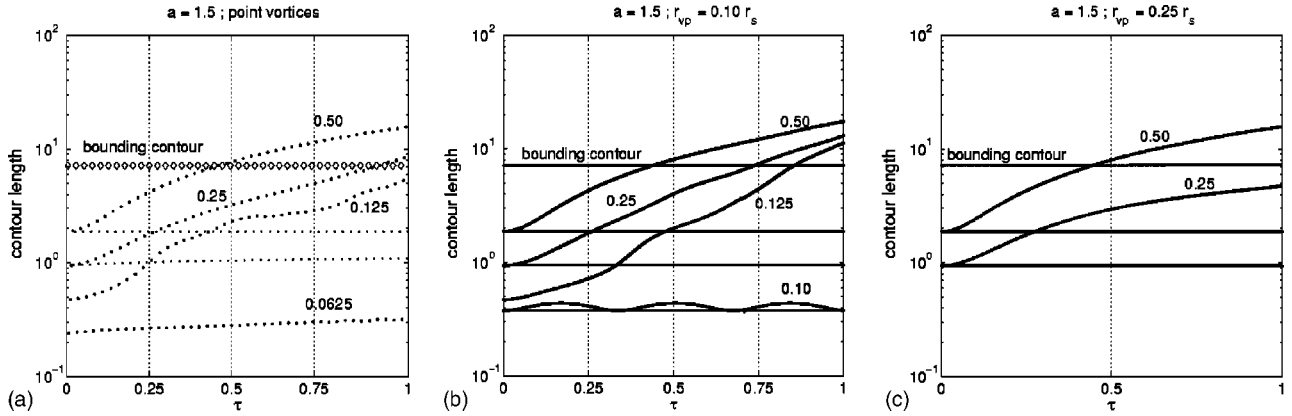

FIG. 9. The contour variation of all passive contours in the tripolar system shown in Fig. 8 with (a) $r_{vp}=0$, (b) $r_{vp}=0.10r_s$, and (c) $r_{vp}=0.25r_s$. The passive contours of the central region are labelled with their respective fraction of r_s. The (virtually) horizontal lines indicate the passive satellite contours and the bounding contour.

The dimensionless simulation time for the numerical experiments is in most runs limited to $\tau=1$, which enabled us to do many experiments in a reasonable amount of time. A few runs have been performed with $\tau>1$ in order to assess numerical inaccuracies, and to see how these may affect the stability of the symmetrical multiple-patch vortices.

A. The tripolar vortex

The tripolar solution is investigated for $a=1.5$ and $a=2$ and six values for r_{vp} (see Table I). The first of these values is $r_{vp}=0$ and designates the generic tripolar equilibrium with point vortices. The end result (at $\tau=1$) of the evolution for $a=1.5$ is shown in Fig. 8(a). This panel clearly shows the strong advection behavior in the central region of the system. In Fig. 9(a) this is further substantiated by plotting the length of all contours in the vortex, i.e., $\log(L_c)$ versus τ. We do, however, observe that the length of the smallest passive contour ($r_{pc}=0.0625r_s$) changes only marginally, while the other three contours in the center are transported throughout the entire vortex structure. The two passive contours in the satellite region show hardly any increase in their length.

The following step is to replace the point vortices with patches and obtain quantitative results for the range of patch radii given above. First we show in Fig. 8(b) the end result of the evolution of the $a=1.5$ vortex (with $r_{vp}=0.10r_s$). An immediate observation is that the system is stable for this regularization. This is remarkable since the results reported by Crowdy and Cloke[8] indicate that the tripolar equilibrium is unstable for linear perturbations. The results of contour length measurements are shown in Fig. 9(b), where the variation of the contours with $r_{pc}\geqslant 0.125r_s$ shows similar behavior as compared to the point-patch vortex. The finite patches have size $r_{vp}=0.10r_s$ and for the central patch the lengthening of its contour shows a pulsating behavior. The patch undergoes a deformation from circular to ellipsoidal and vice versa in a periodic manner. Horizontal lines in both pictures (except for the labelled bounding contour) indicate the passive contours of the satellite region.

The snapshot in Fig. 8(c) shows the final result of the evolution of the same ($a=1.5$) vortex, but now with a patch size $r_{vp}=0.25r_s$. Here the dynamics shows quite a different behavior. The system clearly becomes unstable while the central patch breaks up into two equal-sized pieces, preserving the symmetry of the vortex (note that the perturbations applied to the tripolar system in Sec. II break the symmetry in advance, and that the symmetric perturbations employed by Crowdy and Cloke[8] are contaminated by small numerical errors finally yielding loss of symmetry). The end result is the formation of two dipolar vortices. The length of the contours is given in Fig. 9(c), where it is shown that the contour length of the central patch increases and the vortex becomes unstable.

Next the results for the $a=2$ vortex are given for a patch size $r_{vp}=0.10r_s$. In Fig. 10(a) the final result of the evolution of the system is shown, and the variation of the contour length is displayed in Fig. 11(a). We see an identical behavior for the small central patch when compared to the $r_{vp}=0.10r_s$ vortex with $a=1.5$. The system remains in its original shape, while the central patch deforms only slightly in a pulsating manner. The time period is, however, smaller—as is the increase of length (amplitude of the sinusoidal curve) of the contour. In Fig. 10(b) we have shown the contour plots of vorticity and passive tracer at $\tau=1$ for the run with $a=2$ and $r_{vp}=0.25r_s$, and for the same run the contour lengthening is presented graphically in Fig. 11(b). Like $r_{vp}=0.25r_s$ for the

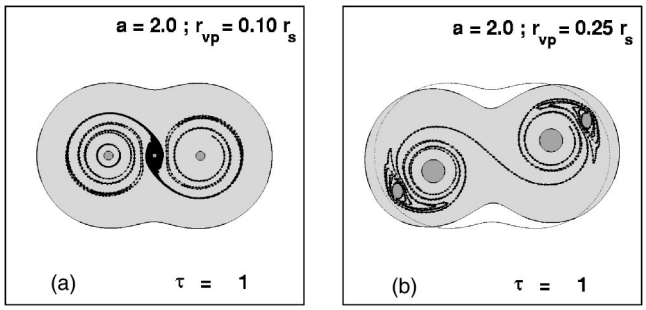

FIG. 10. Snapshots of the evolution of the $a=2.0$ tripolar system ($n=3$) at $\tau=1$ with $r_{vp}=0.10r_s$ (left panel) and $r_{vp}=0.25r_s$ (right panel). The gray and dark gray areas represent the vorticity patches, and the black dots designate the passive tracers.

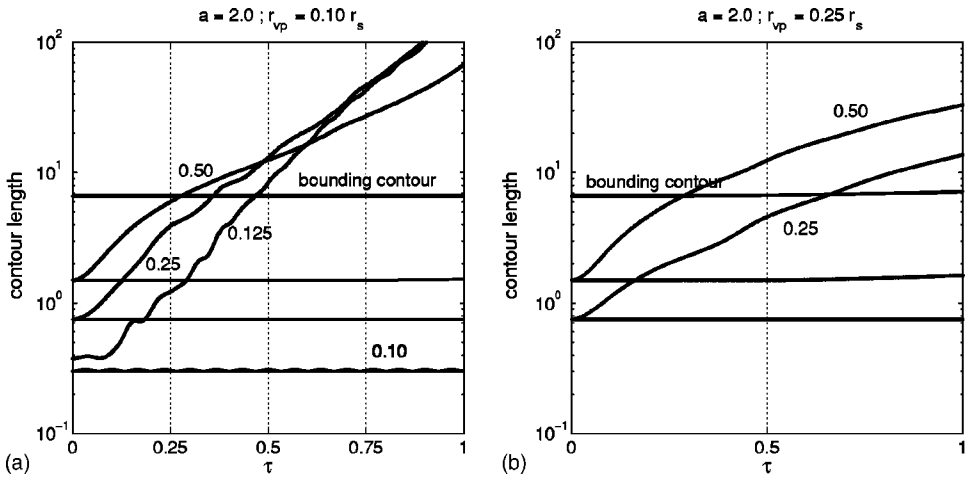

FIG. 11. The contour variation of all passive contours in the tripolar system shown in Fig. 10 with (a) $r_{vp}=0.10r_s$ and (b) $r_{vp}=0.25r_s$. The passive contours of the central region are labeled with their respective fraction of r_s. The (virtually) horizontal lines indicate the passive satellite contours and the bounding contour.

$a=1.5$ system, the vortex is unstable and breaks up into two dipoles. Note that careful inspection of the contour plot reveals that the two dipole halves, originally constituting the central vortex patch, are not disconnected (no contour surgery[10,18] is applied). The contour lengthening, and thus the transport, is more severe than in the $a=1.5$ vortex. Moreover, the outer contour has changed its initial shape considerably. Both aspects are most likely due to the fact that the satellites are closer to each other for larger values of a.

The results presented so far only apply for two values of r_{vp}. Proper choices for other vorticity patch sizes (according to Table I) can yield a better picture for the behavior of the tripolar vortex. The amplification factor A, which was introduced in Eq. (3), will be useful in determining the character of the multiple-patch vortex for many more experiments. The results are shown in Fig. 12 for both the $a=1.5$ and the $a=2$ configuration. In the amplification results, the black-filled circles represent the vorticity patches with their respective radius r_{vp}. The size of the open circles have the same meaning, but then for the passive contours (the largest open circle represents the passive contour with $r_{pc}=0.50r_s$). The results in Fig. 12 clearly indicate that $A=1$ for $r_{vp}=0.10r_s$ for both a. This was already verified with the former contour variation results. We further remark that the amplification in case of the pulsating contour length is normalized to unity when its average is time independent. Moreover, the $a=1.5$ tripolar system is unstable for $r_{vp}\geqslant 0.125r_s$, while for the $a=2$ vortex the system remains stable for r_{vp} at least up to $0.15r_s$. These values represent pulsating contour lengths for the central patch. The behavior of these cases are further highlighted in Fig. 13.

Figure 13(b) shows that the vortex is stable for a long evolution time until a certain moment when the contour length shows a more irregular variation: the vortex becomes unstable. The arrow signatures the moment the outer contour starts to change its shape. This is solely due to numerical inaccuracies, that is, small roundoff errors add up and in the time frame given, resulting in an imbalance in the equilibrium. In Fig. 14 this is further highlighted when the same simulation for different time step sizes is given. Vosbeek[16] has investigated the (lack of) area conservation of several time-integration schemes applied to contour dynamics. In this study it was shown that the area $\mathcal{A}$ of a (circular) patch of uniform vorticity decreases as

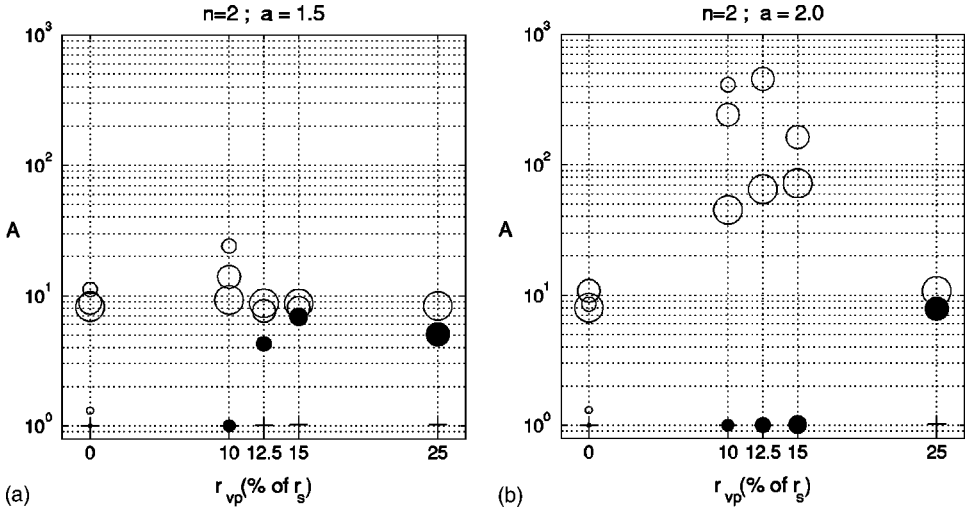

FIG. 12. The amplification factor of all contour lengthening measurements for the tripolar vortex ($n=2$) with $a=1.5$ (left) and $a=2.0$ (right). The open and filled circles represent the amplification factors of the passive contours and the contours of the interior vorticity patches, respectively, and the + designates the amplification factor of the bounding contour. The meaning of the size of the filled circles is given on the horizontal axis. The size of the open circles designates the same patch radii as the filled circles, and the largest open circle represent the case $r_{pc}=0.50r_s$.

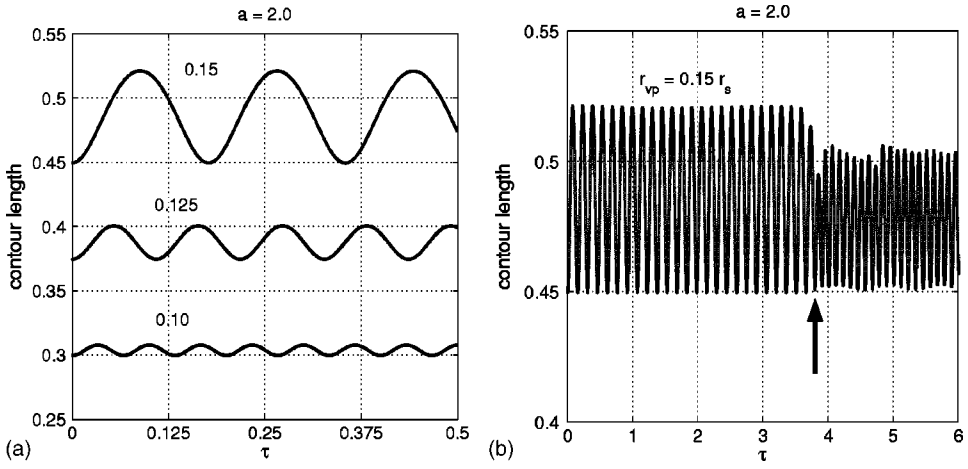

FIG. 13. Graphs illustrating the contour-length evolution of the central patch of the tripolar vortices ($n=2$) with $a=2.0$ and $r_{vp}=0.10$, 0.125, and 0.15. (a) The contour length of three central patch sizes for the tripolar $a=2$ vortex. (b) Long-time evolution for the vortex with $r_{vp}=0.15r_s$.

$$\mathcal{A}(t) \sim \mathcal{A}(0)\, e^{-t(\omega/2)^6(\Delta t)^5/72}, \tag{4}$$

when an explicit fourth-order Runge–Kutta time integration scheme (RK4) is implemented. The same time integration scheme is used in the present simulations. In our multiple-patch vortices, the satellite patches contain the strongest uniform vorticity compared to the other vorticity sources (background patch, central patch) and thus influence the flow simulation significantly when different time steps are used. By increasing the time step, the areas of the satellite patches decrease much faster, as can be deduced from Eq. (4), and alter the flow field in such a way that the bounding contour deforms severely. The small patches (satellites and central patch) wander off from their original positions and the entire vortex becomes unstable. We determine this unstable behavior through the variation in the bounding contour. Figure 14(b) clearly shows the dependence on time step size for the vortex to remain stable. We can state that, in this example with an $r_{vp}=0.15\,r_s$ vortex, the stable tripolar solutions—with pulsating central patch contours—become unstable in the course of time solely due to numerical errors.

The method of replacing each point vortex by a circular patch of equivalent circulation intrinsically imposes certain symmetries on the perturbations. We have also performed several simulations with integration times up to $\tau=2$ with off-center patches (the "center of mass" of the central vorticity patch had a relative displacement of 0.001) and some additional runs with contour perturbations as employed in Sec. II. We have considered the tripolar vortex with $a=1.5$ and $a=2.0$, respectively, each with $r_{vp}=0.10r_s$ and $r_{vp}=0.25r_s$. Both the introduction of off-center patches and contour perturbations promoted the instability of the tripole, which might reasonably well be expected (similar perturbations of Crowdy's tripolar vortex induces instabilities). The simulations clearly indicate that the size of the central and satellite vorticity patches strongly influences the destabilization of the tripolar vortex. The runs with $r_{vp}=0.10r_s$ shows always a deflection of the central vortex towards one of the satellite regions (which one is determined by the details of the perturbation). The other set of simulations, with $r_{vp}=0.25r_s$, reveals that the central vorticity patch breaks up virtually symmetrically (the patches remain connected by a thin vorticity filament). The destabilization of the tripolar vortex seems thus less vigorous for this set of simulations than for the runs with $r_{vp}=0.10r_s$.

B. The triangular vortex

For the numerical experiments of the triangular vortex (see Table II) it is convenient to show the amplification factor for all simulations and pick out two interesting vortex systems for a brief discussion. These two vortices are those

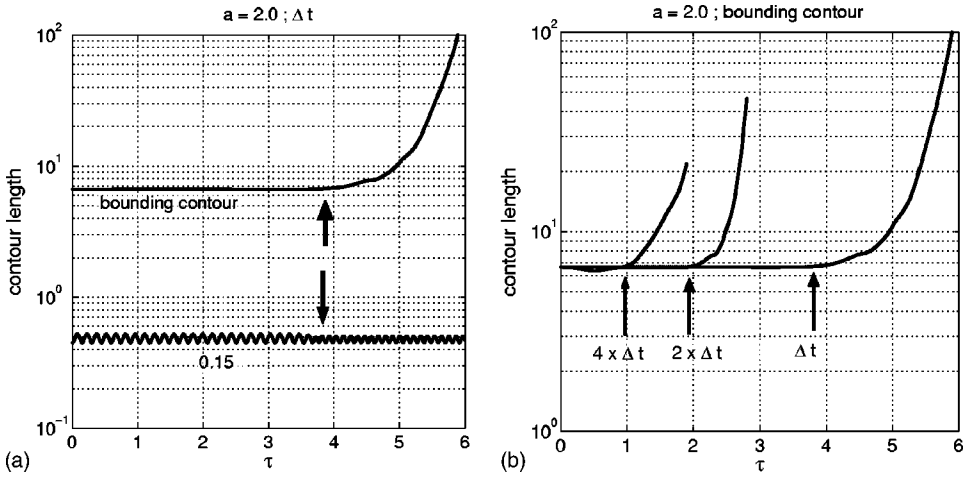

FIG. 14. Graphs illustrating the contour-length evolution of the central patch and the bounding contour of the tripolar vortex ($n=2$) with $a=2.0$ and $r_{vp}=0.15$. (a) The bounding contour and the central patch contour. (b) Three time step sizes mark the difference in unstable behavior of the vortex.

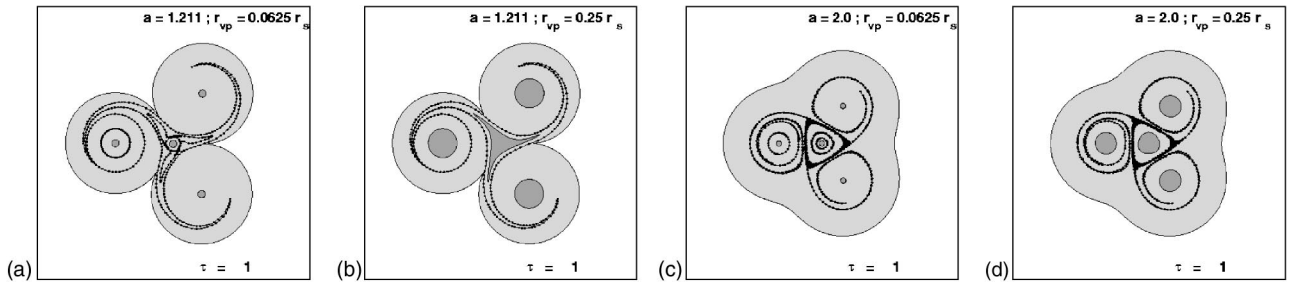

FIG. 15. The end results of the evolution of the triangular ($n=3$) vortex with $a=1.211$ for $r_{vp}=0.0625r_s$ (a) and $r_{vp}=0.25r_s$ (b), and of the $a=2.0$ vortex for $r_{vp}=0.0625r_s$ (c) and $r_{vp}=0.25r_s$ (d).

with $a=1.211$ and $a=2.0$ (the smallest and largest a, respectively, in our numerical experiments). The evolution of the triangular vortex with $a=1.211$ is shown in Figs. 15(a) and 15(b) for the values $r_{vp}=0.0625r_s$ and $r_{vp}=0.25r_s$. A major difference that is immediately observed is the deformation of the central patch in case of the triangular vortex with $r_{vp}=0.25r_s$. A small amount of the vorticity is equally transported into the satellite regions. Apparently, this has no effect on the stable evolution of the vortex, i.e., the outer contour does not deviate from its starting length and position in the course of time, and the (strong) satellite patches remain at their initial positions. Figures 16(a) and 16(b) show the values of the increase in contour length versus time for both r_{vp} simulations. The transport of the outer two passive contours ($r_{pc}=0.25r_s$ and $r_{pc}=0.50r_s$) is similar for both r_{vp} simulations. This can be further verified in Fig. 17 where the amplification for all numerical experiments are given.

Snapshots of the evolution from two experiments of the triangular vortex with $a=2.0$, with $r_{vp}=0.0625r_s$ and $r_{vp}=0.25r_s$, respectively, are illustrated in Figs. 15(c) and 15(d). This vortex shows a similar stable behavior as the $a=1.211$ vortex. However, a big difference is observed in the measurement of the transport of the tracers in the flow. Especially in the outer region of the vortex the $r_{pc}=0.50r_s$ passive contour shows clearly a strong advection throughout the vortex and especially in the central region. The central patch in case of the $r_{vp}=0.0625r_s$ simulation is, as in the $a=1.211$ simulation, not deforming at all, yet the $r_{vp}=0.25r_s$ in this $a=2.0$ simulation shows a small pulsating deformation of the central patch of vorticity, resembling the behavior as seen for the stable tripolar vortex.

Summarizing, all performed simulations show stable triangular vortex systems, be it that the central patch is deformed for the combination of large r_{vp} and small a. This behavior of the central patch differs per r_{vp} value, yet has no effect on the evolution of the vortex as such. This is quite different from the behavior of the tripolar vortex ($n=2$), which is very sensitive to perturbations of its centrally placed vortex for large r_{vp}. Transport of tracers in the flow is stronger for larger a for the region in the flow where the tracers are farthest apart from the embedded (and strong) vorticity patches.

C. The square vortex

Similar to the case of the triangular vortex, the many results for the square vortex (see Table II) requires an efficient approach in order to quantify the properties of transport and stability. Figure 18 shows the amplification factors for the simulations performed with $a=1.241$, 1.39, 1.43, 1.45, 1.5, and 2.0 (for a full overview of the results, see Ref. 12). The value $a=1.4$ was indicative for the separation of stable and unstable regimes through the theory (Crowdy and Cloke[8]) and through the numerical experiments conducted in Sec. II. We highlight, as we did in case of the stable triangular vortex, two multiple-patch vortices for two values of r_{vp}

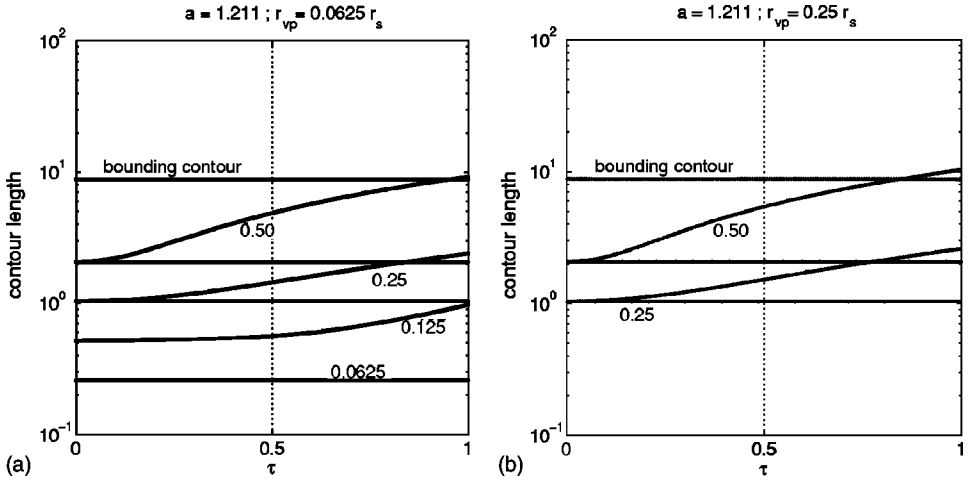

FIG. 16. The contour variation of all passive contours in the triangular vortex with $a=1.211$ (displayed in Fig. 15). The contour length variation for the $r_{vp}=0.0625r_s$ vortex and the $r_{vp}=0.25r_s$ vortex are displayed in (a) and (b), respectively. The passive contours of the central region are labeled with their respective fractions of r_s. The (virtually) horizontal lines indicate the passive satellite contours and the bounding contour.

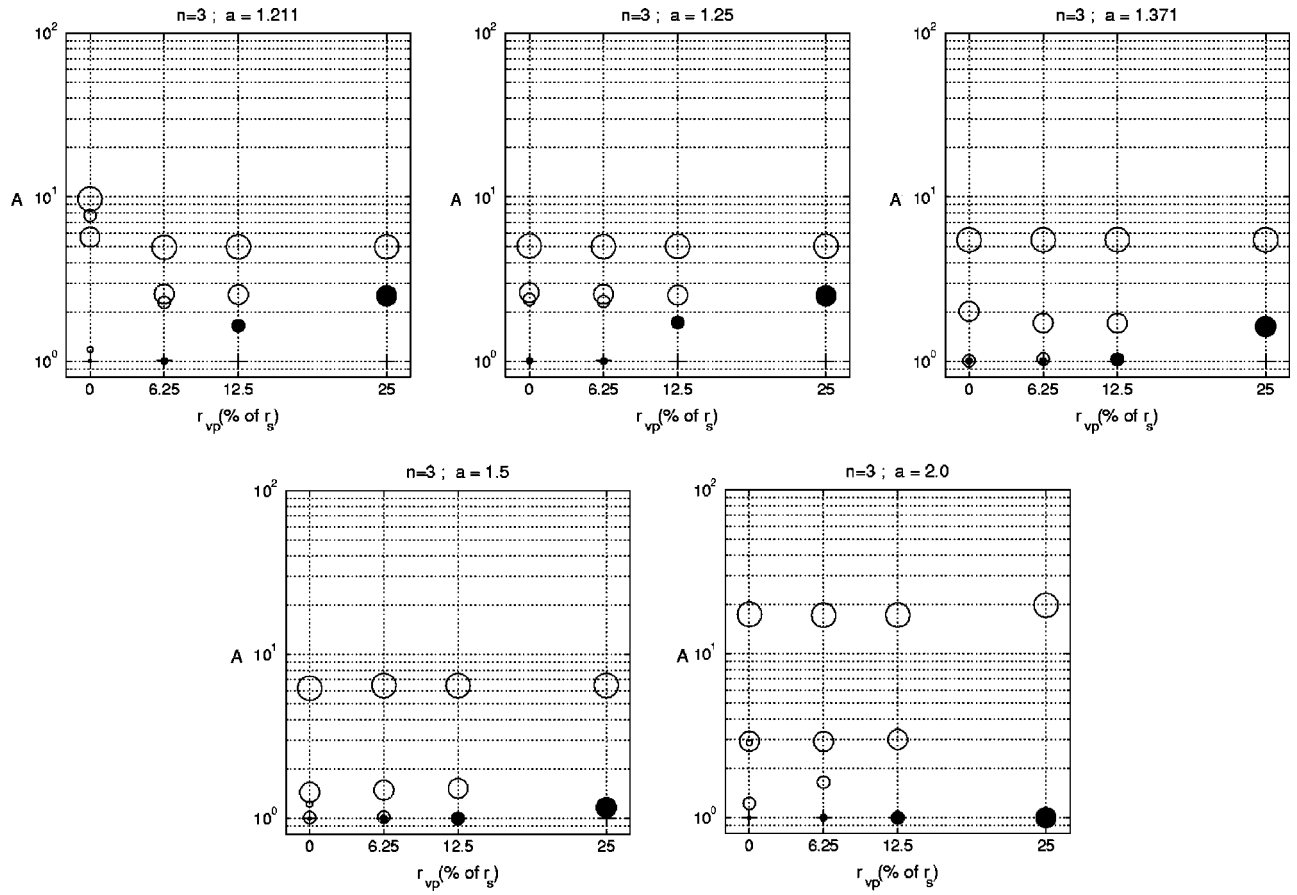

FIG. 17. Amplification factors of the triangular vortex ($n=3$) for all a according to Table II. The open and filled circles represent the amplification factors of the passive contours and the contours of the interior vorticity patches, respectively, and the + designates the amplification factor of the bounding contour. The meaning of the size of the filled circles is given on the horizontal axis. The size of the open circles designates the same patch radii as the filled circles, and the largest open circle represent the case $r_{pc}=0.50r_s$.

each. The $a=1.241$ (smallest possible a) and the $a=1.5$ vortex are compared. The evolution of the $a=1.241$ vortex is shown in Figs. 19(a) and 19(b). The advection of the $r_{pc}=0.50r_s$ contour through the entire vortex is apparent and only for this contour we measure an increase in length [Fig. 20(a)]. The large $r_{vp}=0.25r_s$ evolution is illustrated in Fig. 19(b) and shows a stable vortex with a deformed central patch in the shape of a square. The length of the square central vortex is only marginally increasing, and no pulsating deformation of the square central vortex patch is observed (for $a=1.241$). The outer contour and the position of the satellite patches do not deviate in any way from their initial settings.

The evolution of the $a=1.5$ vortex is given in Figs. 19(c) and 19(d). This vortex should not be in equilibrium according to the theory and the results of the numerical simulations in Sec. II. This is not the case in these multiple-patch vortices. Both r_{vp} simulations show stable vortices (a small pulsating deformation of the central vortex patch is observed) with a similar advection of the passive contour ($r_{pc}=0.50r_s$). The transport is, however, a little stronger compared to the $a=1.241$ vortex, and differs in its growth rate. For the $a=1.5$ experiments it has an exponential growth rate. Again, as in the former $n=2$, $n=3$ multiple-patch systems, the larger a is, the stronger the transport is for tracers in those regions in the flow where they have the largest distance to the patches (always the passive $r_{pc}=0.50r_s$ contour in our study).

The observations and quantitative results for the two vortex systems discussed are further highlighted in the results for the amplification factor in Fig. 18. It is shown that there is not much variation in the flow dynamics for this entire range of a values given in Table II. The square multiple-patch vortices in this study are all stable for the given values of a, although they might be considered as (symmetrically) perturbed multipolar equilibria as introduced by Crowdy.[1]

IV. CONCLUSIONS

A few important conclusions can be drawn from the present investigation. The first one concerns the mixing properties of the fluid nearby the bounding contour of the multipolar vortex equilibria. In particular, there are indications for two distinct regimes of mixing in the otherwise stable triangular vortex equilibria. For $a=1.371$ considerable mixing occurs while mixing is virtually absent in the numerical experiment with $a=2.0$. This issue has been investigated in some more detail for the square vortex equilibria. The stable equilibria ($a \lesssim 1.4$) show substantial mixing of fluid

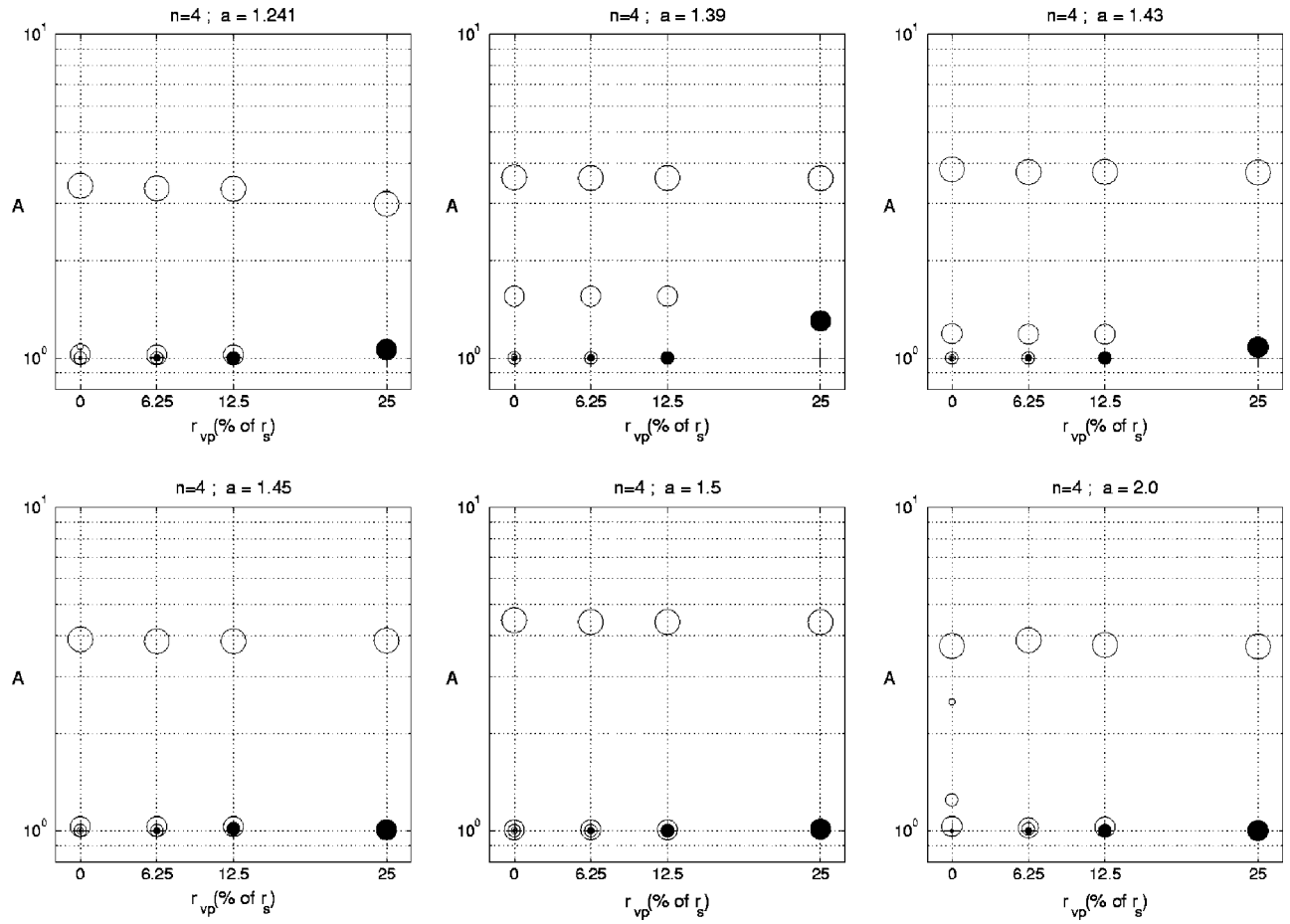

FIG. 18. Amplification factors of the square vortex system ($n=4$) for $a=1.241$, 1.39, 1.43, 1.45, 1.5, and 2.0. The open and filled circles represent the amplification factors of the passive contours and the contours of the interior vorticity patches, respectively, and the + designates the amplification factor of the bounding contour. The meaning of the size of the filled circles is given on the horizontal axis. The size of the open circles designates the same patch radii as the filled circles, and the largest open circle represent the case $r_{pc}=0.50r_s$.

initially located near the edge of the vortex, while any substantial mixing of these fluid elements is absent for the unstable square vortex equilibria. For the simulations with the multiple-patch systems it appears that mixing is strong for fluid elements initially located near the central vortex, while passive contours are less, or virtually not, affected when situated nearby the satellite patches.

Another important conclusion concerns the stability of the symmetrical multiple-patch systems, which we consider as slightly perturbed multipolar equilibria as introduced by Crowdy.[1] Surprisingly, the tripolar system is stable (in the sense that the tripole will survive as a coherent structure) provided the patch size is less than a critical value which depends on the value of a. Interestingly, when the patch size is less than this criticial value the multiple-patch tripolar quasiequilibrium exhibits oscillations of an ellipsoidal kind of the central vortex patch, and is thus unsteady. For $a=1.5$ stability is observed for $r_{vp}\leqslant 0.1r_s$, and for $a=2.0$ stability is observed for $r_{vp}\leqslant 0.15r_s$. The tripolar equilibrium as introduced by Crowdy is unstable (in the sense that the tripole is destroyed) for any perturbation of the point vortex positions, strength variations of the vorticity, and the position of the

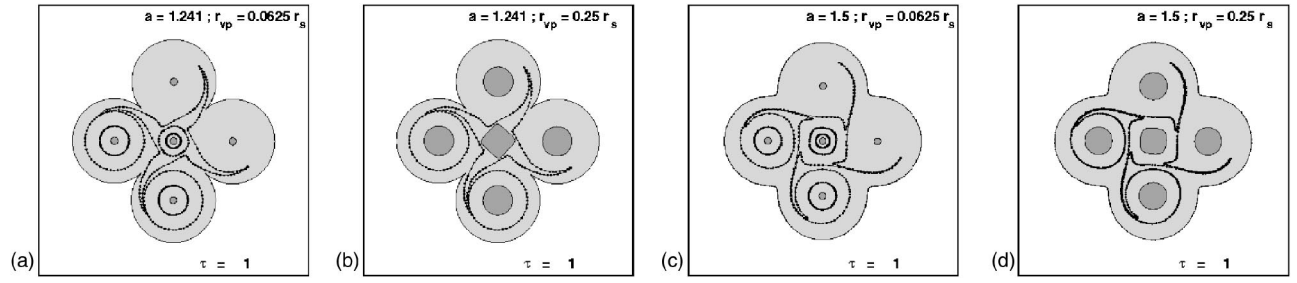

FIG. 19. The end results of the evolution of the square ($n=4$) vortex with $a=1.241$ for $r_{vp}=0.0625r_s$ (a) and $r_{vp}=0.25r_s$ (b), and of the $a=1.5$ vortex for $r_{vp}=0.0625r_s$ (c) and $r_{vp}=0.25r_s$ (d).

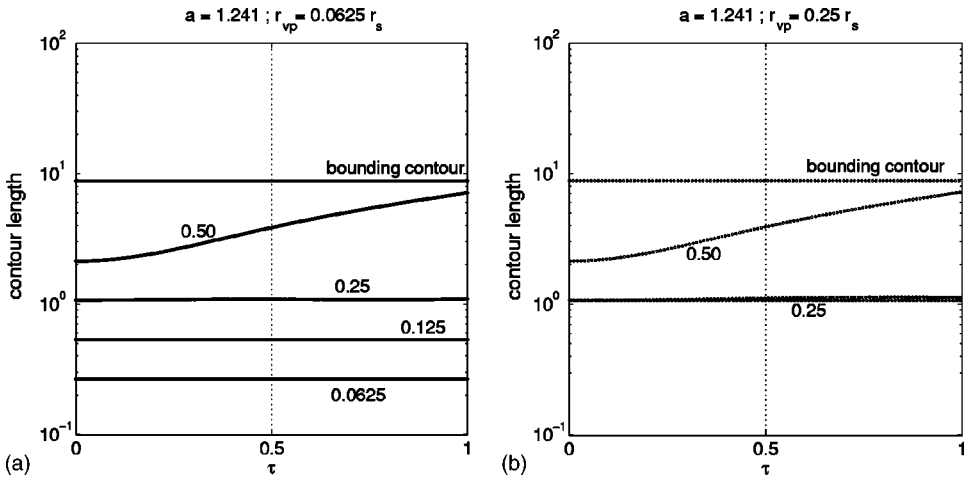

FIG. 20. The contour variation of all passive contours in the square vortex with $a=1.241$ (displayed in Fig. 19). The contour length variation for the $r_{vp}=0.0625r_s$ vortex and the $r_{vp}=0.25r_s$ vortex are displayed in (a) and (b), respectively. The passive contours of the central region are labelled with their respective fractions of r_s. The (virtually) horizontal line without label in (b) indicate the passive satellite contour with $r_{pc}=0.25r_s$. The other satellite contours are virtually indistinguishable from the passive tracer contours in the central region.

bounding contour. The triangular-patch vortex remains stable, despite the strong deformation of the central vortex patch, and all square vortices considered in this study remain stable.

These numerical observations will hopefully initiate more detailed analytical stability studies of these multipolar-patch systems to elucidate the criteria for stability. Moreover, (numerical) stability studies should include a sufficiently broad class of disturbances, including those which will break symmetry of the regularized Crowdy vortices, in order to assess to agreement with the stability properties of the exact multipolar equilibria introduced by Crowdy.

ACKNOWLEDGMENTS

This work was sponsored by the Stichting Nationale Computerfaciliteiten (National Computing Facilities Foundation, NCF) for the use of supercomputer facilities, with financial support from the Netherlands Organization for Scientific Research (NWO).

APPENDIX

In this appendix we provide a brief description to obtain exact steady solutions of the 2D Euler equations with n-fold symmetry as reported by Crowdy.[1,19]

From complex function theory it is known that a unit circle in a complex parametric ξ plane can be mapped onto a curve in the complex z plane and vice versa. The curve in the z plane then represents the bounding contour of the vortex. Likewise, the interior of the unit disk can be mapped onto the interior of the vortex in a single valued way. Transformations for which the unit disk with more than one embedded singularity is mapped into the physical plane, have the following form for any integer $n \geqslant 2$:

$$z(\xi) = R\xi\left(1 + \frac{b}{\xi^n - a^n}\right). \tag{A1}$$

This mapping constitutes vortex patches with $n+1$ embedded point vortices. This vortical configuration has one central point vortex and n satellite point vortices and constitutes a dynamical equilibrium. The parameters a, b, and R are real, whereas b can be found when both a and n are given (see Refs. 1,19). The parameter R is an arbitrary normalization parameter that determines the size of the vortex patch. Thus the parameters n and a determine the mapping for $n \geqslant 2$ and $a \geqslant 1$. Note, however, that the value for a specifies the position of $n-1$ poles (the satellite extrema) inside the unit circle in the ξ plane. Its value is, however, special for each n.

We require that each point vortex is steady. This is achieved by expanding the velocity field around each singular point by means of a Laurent expansion in z. The constant in each expansion is set to zero, implying steadiness, resulting in the determination of the strength Γ of the point vortex (Crowdy[1]). The locations of the point vortices in the z plane are determined by putting the simple poles in the ξ plane at

$$\xi = \frac{1}{a}\, e^{2\pi i(k-1)/n} \quad \text{for} \quad k = 1,2,\ldots,n. \tag{A2}$$

The parameter R is then appropriately determined by specifying the area A of the vortex patch. The total circulation is zero and this can be seen by adding the circulations of the patch and all n point vortices: $\Gamma_P + \Gamma_c + n\Gamma_s = 0$. Here, $\Gamma_P = \omega A$ is the circulation of the patch with given area A and uniform vorticity ω, and Γ_c, Γ_s are the circulations of the central point vortex and satellite point vortex, respectively.

As an illustration we consider the tripole ($n=2$). For $n=2$ we have the conformal mapping

$$z(\xi) = R\xi\left(1 + \frac{b}{\xi^2 - a^2}\right) \tag{A3}$$

with accompanying schematic in Fig. 21. The associated Schwarz function is given as

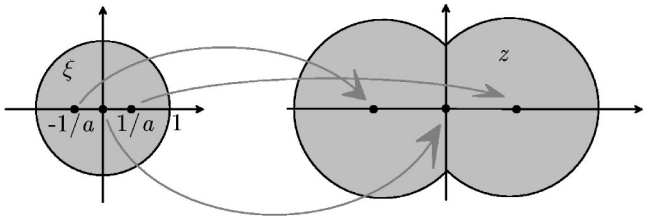

FIG. 21. Schematic of the mapping of a unit circle from the parametric plane onto a physical shielded tripolar vortex.

$$S[z(\xi)] = \frac{R}{\xi}\left(1 + \frac{b\,\xi^2}{1 - a^2\xi^2}\right), \tag{A4}$$

and indicates the point vortex in the origin of the physical plane, whereas $\xi = \pm 1/a$ designates the two satellite coordinates.

[1] D. Crowdy, "A class of exact multipolar vortices," Phys. Fluids **11**, 2556 (1999).
[2] D. A. Schecter, D. H. E. Dubin, K. S. Fine, and C. F. Driscoll, "Vortex crystals from 2D Euler flow: Experiment and simulation," Phys. Fluids **11**, 905 (1999).
[3] D. Durkin and J. Fajans, "Experiments on two-dimensional vortex patterns," Phys. Fluids **12**, 289 (2000).
[4] D. Durkin and J. Fajans, "Experimental dynamics of a vortex within a vortex," Phys. Rev. Lett. **85**, 4052 (2000).
[5] M. Amoretti, D. Durkin, J. Fajans, R. Pozzoli, and M. Romé, "Asymmetric vortex merger: Experiments and simulations," Phys. Plasmas **8**, 3865 (2001).
[6] D. Z. Jin and D. H. E. Dubin, "Point vortex dynamics within a background vorticity patch," Phys. Fluids **13**, 677 (2001).
[7] K. S. Fine, A. C. Cass, W. G. Flynn, and C. F. Driscoll, "Relaxation of 2D turbulence to vortex crystals," Phys. Rev. Lett. **75**, 3277 (1995).
[8] D. Crowdy and M. Cloke, "Stability analysis of a class of two-dimensional multipolar vortex equilibria," Phys. Fluids **14**, 1862 (2002).
[9] N. J. Zabusky, M. H. Hughes, and V. K. Roberts, "Contour dynamics for the Euler equations in two dimensions," J. Comput. Phys. **30**, 96 (1979).
[10] D. G. Dritschel, "Contour dynamics and contour surgery: Numerical algorithms for extended high-resolution modelling of vortex dynamics in two-dimensional, inviscid, incompressible flows," Comput. Phys. Rep. **10**, 77 (1989).
[11] G. K. Morikawa and E. V. Swenson, "Interacting motion of rectilinear geostrophic vortices," Phys. Fluids **14**, 1058 (1971).
[12] R. M. Schoemaker, "Contour dynamics for vortex-induced advection," Ph.D. thesis, Eindhoven University of Technology, Eindhoven, The Netherlands, 2003.
[13] G. K. Batchelor, *An Introduction to Fluid Mechanics* (Cambridge University Press, Cambridge, 1967).
[14] H. Aref, "Integrable, chaotic, and turbulent vortex motion in two-dimensional flows," Annu. Rev. Fluid Mech. **15**, 345 (1983).
[15] D. I. Pullin, "Contour dynamics methods," Annu. Rev. Fluid Mech. **24**, 89 (1992).
[16] P. W. C. Vosbeek, "Contour dynamics and applications to 2D vortices," Ph.D. thesis, Eindhoven University of Technology, Eindhoven, The Netherlands, 1998.
[17] P. W. C. Vosbeek, H. J. H. Clercx, and R. M. M. Mattheij, "Acceleration of contour dynamics simulations with a hierarchical-element method," J. Comput. Phys. **161**, 287 (2000).
[18] D. G. Dritschel, "Contour surgery: a topological reconnection scheme for extended integrations using contour dynamics," J. Comput. Phys. **77**, 240 (1988).
[19] D. Crowdy, "Multipolar vortices and algebraic curves," Proc. R. Soc. London, Ser. A **457**, 2337 (2001).